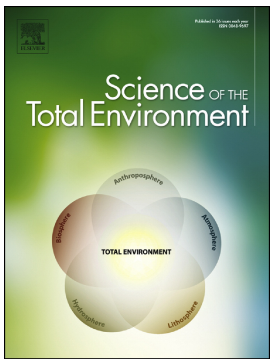

Quantifying the influences of natural and human factors on the water footprint of afforestation in desert regions of northern China

Ziyu Wang, Duanyang Xu, Daoli Peng, Yue Zhang

PII: S0048-9697(21)01645-4

DOI: https://doi.org/10.1016/j.scitotenv.2021.146577

Reference: STOTEN 146577

To appear in: *Science of the Total Environment*

Received date: 23 January 2021

Revised date: 11 March 2021

Accepted date: 15 March 2021

Please cite this article as: Z. Wang, D. Xu, D. Peng, et al., Quantifying the influences of natural and human factors on the water footprint of afforestation in desert regions of northern China, *Science of the Total Environment* (2021), https://doi.org/10.1016/j.scitotenv.2021.146577

Quantifying the influences of natural and human factors on the water footprint of afforestation in desert regions of northern China

Ziyu Wang[a,b], Duanyang Xu [a, *], Daoli Peng [b, * *], Yue Zhang[a]

[a] Key Laboratory of Land Surface Pattern and Simulation, Institute of Geographic Sciences and Natural Resources Research, Chinese Academy of Sciences, Beijing 100101, China; [b] College of Forestry, Beijing Forestry University, Beijing 100083, China.

[*] Corresponding author.

Email: xudy@igsnrr.ac.cn (D. Xu)

[* *] Co-corresponding author.

Abstract: To mitigate desertification and alleviate soil erosion, a wide range of ecological restoration initiatives have been implemented in arid and semi-arid areas, the water consumption of ecological projects and driving mechanisms received increasing attention to balance economy development and ecology restoration at different scales. In this study, the water footprint (WF) was employed as an indicator of water consumption by afforestation, and trend analysis, texture classification and geographical detector methods were used to identify the afforestation area and assess the influences of natural and human factors on the afforestation WF in the desert regions of northern China. The results revealed four major findings. (1) The afforestation area increased by 73,764.31 km^2, from 2003 to 2017, accounting for 2.42% of the study area. (2) On average, the afforestation WF increased from east to west, ranging from 0 to 58.9 m^3/gC, indicating its high spatial heterogeneity. (3) Potential evapotranspiration was the dominant factor influencing the afforestation WF, explaining 20.4% of the variation in afforestation WF. (4) The explanatory power of

natural and human factors was disparate at the different scales and the interactions between different factors had higher impact than that of single factors. These findings could provide valuable information to support more sustainable ecological restoration science and interventions in arid and semi-arid areas.

Keywords: afforestation; water footprint; influencing factors; geographical detector; arid and semi-arid areas

1 Introduction

Desertification is a serious environmental issue that globally causes 120,000 km^2 of productive land to become barren and leads to losses of 20 million tons of grain production every year (UNCCD, 2017). Currently, economic losses caused by desertification are estimated at $50 billion annually and more than 2.7 billion people are threatened by drought and desertification impacts (IPBES LDR, 2018). To combat desertification, a series of ecological projects that mainly rely on afforestation have been implemented worldwide, such as the Great Green Wall Project in Sahel (Ellison and Ifejika Speranza, 2020), the National Action Program in Iran (Amiraslani and Dragovich, 2011), and the New York Declaration on Forests (Bastin et al., 2019). In China, especially, large-scale afforestation projects have been implemented since the 1970s, such as the Three North Shelterbelt Project (TNSP), Natural Forest Protection Project (NFPP) and the Grain for Green Project (GGP), which not only slowed desertification and its expansion in China but also made great contributions to the world's 'greening' trend (Chen et al., 2019; Yuan et al., 2014; Zhang et al., 2020).

Afforestation could significantly improve ecosystem services at the regional level (Barry et al., 2014), especially in arid and semi-arid regions that have undergone

desertification, by controlling soil erosion (Chen et al., 2016), enhancing carbon sink of soil-vegetation systems, and maintaining biodiversity (Liu et al., 2019; West et al., 2020). Meanwhile, the imbalance between forests' water consumption and regional water resources has garnered more attention (Cao and Zhang, 2015; Ma et al., 2013). Previous studies showed that afforestation and other ecological projects in arid and semi-arid regions could actually aggravate the shortage of water resources there (Lu et al., 2018; Xiao et al., 2020). Firstly, afforestation can increase local evapotranspiration and shift the balance of energy and radiation, thereby driving declines in groundwater and soil water storage (Kirschbaum et al., 2011; Liu et al., 2018; Yang et al., 2015). Secondly, afforestation's water consumption may disrupt regional water balance dynamics, as afforestation consumes water resources that would be otherwise be available to support agriculture and other land uses, thus representing an ecological risk at the regional scale (Cao et al., 2016; Zheng et al., 2016).

The determination of water consumption by afforestation and its influencing factors is helpful for figuring out the spatiotemporal differences in water consumption and for optimizing how afforestation is distributed. To measure afforestation's water consumption, previous studies calculated the evapotranspiration rates of afforestation sites for comparison with those of natural vegetation sites (Schwarzel et al., 2020; Tie et al., 2018); other studies have examined differences in soil water contents and depth between afforestation and other land-use types (An et al., 2017; Cao et al., 2018). Although much research has evaluated the water consumption by afforestation and its impact on regional water resources, some limitations persist, namely the lack of spatially explicit analyses and an analysis of the forces driving afforestation's water consumption. The water footprint (WF) is an important indicator of water use and can be used to quantify the total water consumption that occurs to produce given goods

and/or services (Hoekstra, 2003). The calculation of WF in prior studies could thus provide useful guidance for rigorously assessing the water consumption by afforestation (D'Ambrosio et al., 2018; Novoa et al., 2019). The WF framework classifies water consumption into three categories: green WF (water consumed from precipitation), blue WF (water consumed from surface and groundwater), and grey WF (water required to assimilate pollution) (Lovarelli et al., 2016); they are widely used to assess the impact of agricultural production and human lifestyles on local water resources (Ma et al., 2020; Wahba, 2021). On the basis of WF's calculation, several scholars sought to evaluate the sustainability of agriculture and environment, highlighting implications for promoting water use efficiency at different scales (Chouchane et al., 2015; Fan et al., 2019). Yet comparatively little research has assessed afforestation's WF (hereon AWF) in desertified areas at the national scale, with even less attention paid to the influences of different natural and human factors and their potential interactions upon AWF.

To resolve the above problems, we selected the desert regions of northern China and analyzed their AWF and driving mechanism by using the geographical detector model (Wang and Xu, 2017). It quantifies the influence of single factors and their interactions on the dependent (response) variables, and this model has been widely used to analyze the driving forces of diseases, air pollutions, changing landscape patterns, and urban forest distributions, among others (Duan and Tan, 2020; Huang et al., 2014; Liang and Yang, 2016; Wu et al., 2020). The objectives of this work were threefold: (1) to identify the area under afforestation during 2003–2017 across the entire desert region of northern China; (2) to calculate and analyze the AWF; and (3) to quantitatively analyze the impact of different factors upon AWF. This work aims to discern and describe implications for policymakers when devising sustainable

ecological restoration strategies and projects.

2 Materials and method

2.1 Study area

The desert regions of northern China are found across semi-humid, semi-arid, and arid zones, including the landscapes of Inner Mongolia, Xinjiang, Qinghai, Ningxia, Gansu, Hebei, Shanxi, Shaanxi, and Sichuan (31–51°N, 76–125°E). These desert regions encompass a total area of 3.04 million km^2, accounting for 31.46% of China's entire territory. Annual rainfall gradually decreases from east to west, ranging from 0 to 450 mm, and the average temperature is approximately 7°C, with an average annual sunshine duration of 2930 h and annual wind speed of 2.5 m/s. The soil types here mainly include desert soil, saline soil, and semi-hydrated soils. The vegetation coverage in the study area is generally poor, and the dominant species include various shrubs, such as *Haloxylon ammodendron*, *Haloxylon persicum* and *Artemisia ordosica* (Zhu et al., 2015). To address land degradation and improve the environment, many ecological restoration projects were implemented in these desert regions, such as TNSP and Returning Farmland to Forest (Wang et al., 2010a). Under the TNSP, afforestation has reached 26.47 million hm^2, covering most of North, Northwest, and Northeast China (Xie et al., 2020). To better analyze the regional variation, based on the differing natural geographical environment and related research (Xu and Li, 2020), the study area was divided into three desert areas: Inner Mongolia and regions along the Great Wall (IMGW), the arid region of Northwest China (ARNC), and the Three-River Headwaters Region (TRHR). Further, the IMGW and the ARNC were subdivided into 9 and 10 subregions, respectively (Fig. 1, Table A.1).

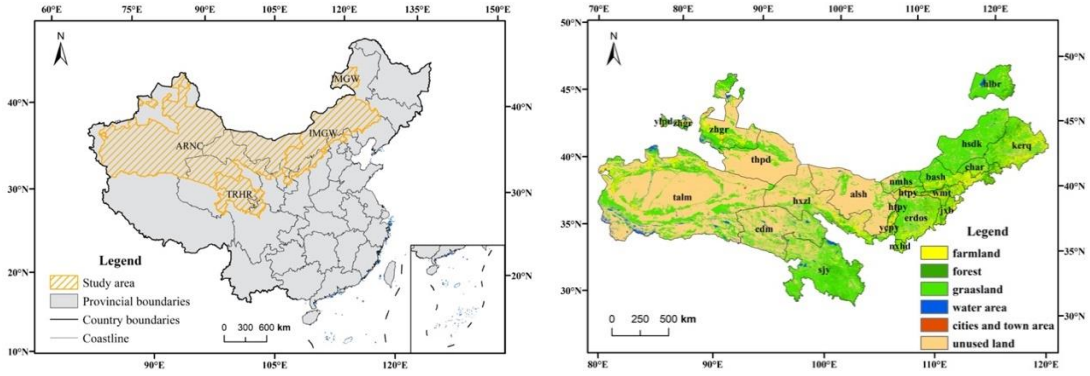

(a) Schematic map of the study area (b) Subregions and main land uses of the study area

Fig. 1. Location of the study area in northern China.

2.2 Data source and preprocessing

The data used in this paper included Landsat data in addition to climate, soil, digital elevation model (DEM), net primary production (NPP), and land cover data as well as some other socio-economic data. The surface reflectance (SR) products of Landsat 5 TM, Landsat 7 ETM+, and Landsat 8 OLI/TIRS were obtained from Google Earth Engine (GEE) (https//earthengine.google.com/). Overall, 19,925 scenes as Landsat images were acquired from 2003 to 2017 by Landsat 5, 7, and 8. To minimize the effects of clouds and cloud shadows, a cloud algorithm (https://developers.google.com/earth-engine/landsat) based on the SR quality assessment bands was used to mask clouds present in the images. The precipitation, temperature, and vegetation evaporation at a 1-km resolution were derived from National Tibetan Plateau Data Center (http://data.tpdc.ac.cn), while the wind speed, potential evaporation, and NPP at a 100-m spatial resolution came from GEE. The DEM data and 1:1,000,000 geomorphic types in China with 1-km spatial resolution were derived from the Data Center for Resources and Environmental Sciences and the Data Center of the Chinese Academy of Sciences (RESDC, http://www.resdc.cn). The soil types (spatial resolution: 1 km) were extracted from a dataset of soil characteristics for China (RESDC). In addition, socio-economic data in the form of

gross domestic product (GDP), human population from 2000 through 2015, and road data at a 1-km spatial resolution were all obtained from RESDC. The land cover data of 2017 (30-m resolution) were derived from Tsinghua University global land cover data (http://data.ess.tsinghua.edu.cn/). To facilitate the spatial analysis and regional comparison, all the data were uniformly converted to 100-m × 100-m grid data.

2.3 Methods

2.3.1 Afforestation extraction

The identification of afforestation is an important prerequisite for this study. Compared with the relatively stable phenological characteristics of natural forest ecosystems, the Normalized Difference Vegetation Index (NDVI) of afforestation areas always show a marked trend of temporal increase due to the positive artificial disturbance involved (Beck et al., 2006; Prabakaran et al., 2013). So, to extract the afforestation areas in the GEE, we used these three steps (Fig. 2):

(1) Extract the area(s) with a significantly increasing trend of NDVI during the 2003–2017 period, by using the trend analysis method. The NDVI values were calculated by using the SR products. The linear slope ($p < 0.05$) was used to identify the NDVI changed significantly from 2003 to 2017 (Eq. 1). A significant, positive slope indicates a greening trend, and a significant but negative slope indicates a browning trend.

$$slope = \frac{n \times \sum_{j=1}^{n}(j \times NDVI_j) - \sum_{j=1}^{n} j \sum_{j=1}^{n} NDVI_j}{n \times \sum_{j=1}^{n} j^2 - \left(\sum_{j=1}^{n} j\right)^2} \quad (1)$$

Where, n is the number of monitoring years, and $NDVI_j$ is the annual maximum NDVI of year j; in the case of a $slope > 0$, this indicates the NDVI has a tendency of increasing.

(2) Identify the regions with forest cover in 2017 by using texture classification

algorithm. The Landsat 8 images from 2017 were used as the primary input data for classifying the most recent land cover types in northern China. For this, 147 samples were collected from Tsinghua University global land cover data set, and another 313 samples from Google Earth. All these samples were uploaded to GEE; 80% of them were randomly selected for training and the remaining 20% reserved as sampling points for validation. Finally, five land use types: forest, grassland, urban, water, and unused land were classified.

(3) Extract afforestation area by overlapping the results derived in the prior two steps. Based on the NDVI trend analysis and the texture classification, the areas of forest cover in 2017 that featured a significant increase of NDVI were identified as having undergone afforestation during 2003–2017.

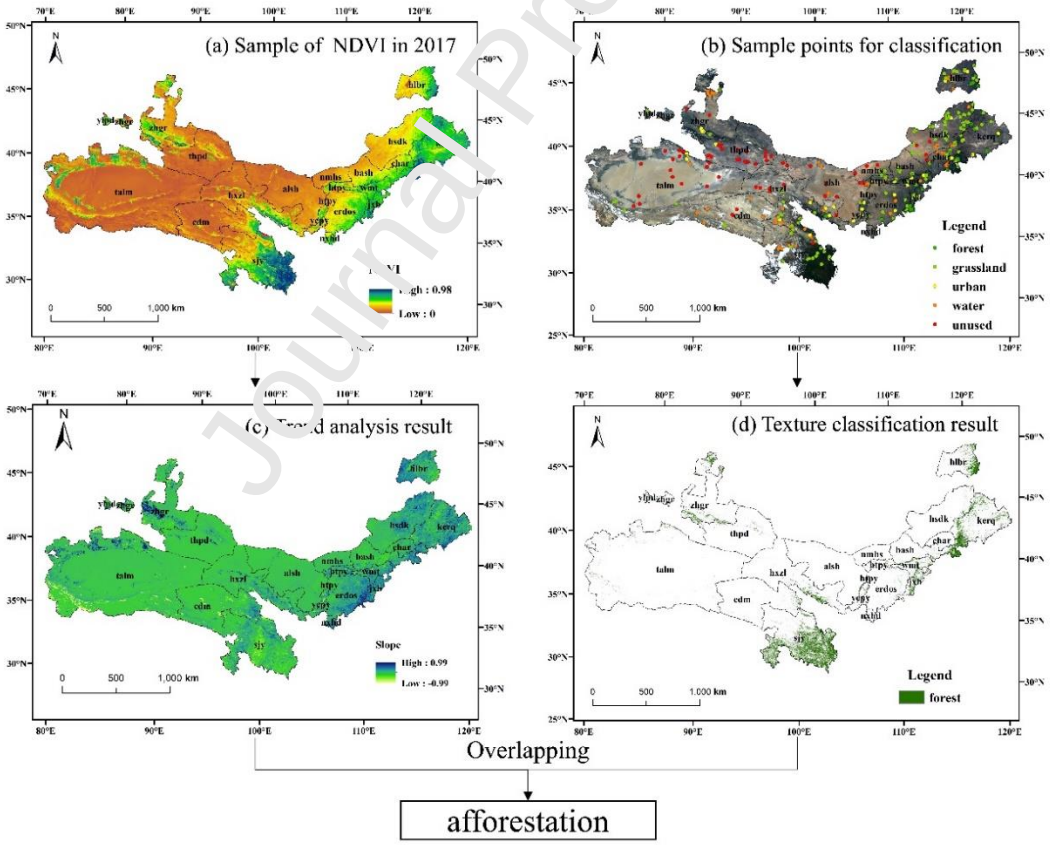

Fig. 2. The workflow of afforestation extraction

2.3.2 AWF calculation

Presuming no fertilizer was used in afforestation, in this study the AWF was calculated as the sum of green WF and blue WF (Bocchiola et al., 2013). For this, methodology proposed by Hoekstral et al. (2011) was followed.

$$WF_{total} = WF_{green} + WF_{blue} \quad (2)$$

where, WF_{total} is the summed AWF (m^3/gC); WF_{green} is the green WF (m^3/gC), which refers to the volume of precipitation used for vegetation growth; WF_{blue} is the blue WF (m^3/gC), which refers to the surface or groundwater used for production purposes.

Both the green (WF_{green}) and blue water footprints (WF_{blue}) of afforestation were determined this way:

$$WF_{green,blue} = \frac{CWU_{green,blue}}{Y} \quad (3)$$

$$CWU_{green,blue} = 10 \times \sum_{d=1}^{lgp} ET_{green,\ blue} \quad (4)$$

where, Y (gC/m^2) is the net primary production of afforestation; $CWU_{green,blue}$ (m^3/m^2) is the green and blue water use, respectively; Σ refers to the annual accumulation of green and blue evapotranspiration; $ET_{green,\ blue}$ are the green and blue water evapotranspiration (mm/year). The factor 10 converts the water depths in millimeters into water volumes per land surface area, expressed in $m^3\ ha^{-1}$.

$$ET_{green} = \min\left(ET_c, P_{eff}\right) \quad (5)$$

$$ET_{blue} = \max\left(0, ET_c - P_{eff}\right) \quad (6)$$

where, ET_c is the vegetation evapotranspiration (mm) and P_{eff} is the effective precipitation (mm) as calculated by the Soil Conservation Service Method developed

by U.S. Department of Agriculture (USDA) (FAO, 2010).

2.3.3 Quantitative analysis the impact of different factors on AWF

(1) Indicator system

The growth of and water consumption by vegetation are closely related to different natural and human factors (Hua et al., 2017). Climate factors (i.e., precipitation, temperature, moisture) will shape the hydrothermal conditions of vegetation growth, thus influencing the amount and extent of water consumption under afforestation. Other natural factors (i.e., soil types, elevation) could reflect the environmental context for vegetation's water consumption. The convenience of transportation as well as economic development can influence the implementation of afforestation and water consumption in the region (Zhang et al., 2018). Therefore, to convey the possible influence of human activities, the GDP, population, and distance from county and road served as the human-related factors in the analysis.

In this study, 12 factors were chosen to discern the effect of different factors on AWF in desert regions of northern China (Table 1). Since the geographical detector is only suitable for discrete variables, all the continuous variables had to be stratified by applying the natural breakpoint method using ArcGIS, version 10.3, mapping software (Esri, Redlands, CA). Besides, soil types and geomorphic types comprised 12 and 6 types, respectively. Detailed information of all factors' classification can be found in appendix information (Fig. A.2).

Table 1 The assessed factors in the study area.

Types	Factor	Code	Units	Classes/types
Natural factors	Average annual precipitation	prec	mm	6
	Annual average temperature	temp	℃	6
	Moisture index	im	class	6

	Annual average wind speed	ws	m/s	6
	Average Annual potential evapotranspiration	pet	mm	6
	Geomorphic types	gmt	categorical	7
	Soil types	soil	categorical	12
	Elevation	dem	m	6
	Gross Domestic Production	GDP	10 000/km^2	6
Human factors	Population	pop	people/km^2	6
	Distance from county	dfc	km	4
	Distance from road	dfr	km	4

(2) Geographical detector

The geographical detector was used to analyze the factors influencing the AWF and the interactions among them. This detector model consisted of four sections, namely, a factor detector, interaction detector, risk detector, and ecological detector (Wang and Xu., 2017).

The factor detector characterized the respective influence of these factors on the AWF by q-value, q∈[0,1]. The q-value indicates the explanatory power of each factor; its power is stronger as the q-value approaches 1. The calculation model to derive q is as follows:

$$q = 1 - \frac{\sum_{h=1}^{L} N_h \sigma_h^2}{N\sigma^2} \quad (7)$$

where, h (1, …, L) is the number of stratifications of a given factor X; N_h and N are the number of units in class h and the whole area, respectively; σ_h^2 and σ^2 are the variance of Y for the units in class h and the whole area, respectively.

The interaction detector can be used to identify whether the interactions of different factors ($X_1 \cap X_2$) are weakened, enhanced, or influence Y independently. The

types of interactive influences are listed by comparing the q-value of the interacting factors to each of the two involved factors, as listed in Table 2.

Table 2 Interaction types of two factors.

Description	Interaction
$q(X_1 \cap X_2) < \text{Min}(q(X_1), q(X_2))$	Weaken; univariate
$\text{Min}(q(X_1), q(X_2)) < q(X_1 \cap X_2) < \text{Max}(q(X_1), q(X_2))$	Weaken; univariate
$q(X_1 \cap X_2) > \text{Max}(q(X_1), q(X_2))$	Enhanced, bivariate
$q(X_1 \cap X_2) = q(X_1) + q(X_2)$	Independent
$q(X_1 \cap X_2) > q(X_1) + q(X_2)$	Nonlinearly enhanced

The risk detector is used to determine whether there is a significant difference in mean values of *Y* between the two subzones of factors and to find those subzones with the highest mean value of *Y*, tested with the *t* statistic (Eq.8). A similar risk detector is often used to detect areas at risk of disease outbreaks and to identify subzones with the highest incidence of different contributing factors (e.g., Wang et al., 2010b).

$$t_{\bar{y}_{h-1}\bar{y}_{h-2}} = \frac{\bar{Y}_{h=1} - \bar{Y}_{h=2}}{\left[\frac{Var(\bar{Y}_{h-1})}{n_{h-1}} + \frac{Var(\bar{Y}_{h-2})}{n_{h-2}}\right]^{1/2}} \quad (8)$$

Where, $\bar{Y}_h$ denotes the average value of *Y* in the subregion *h*; n_h is the sample size in subregion *h*; and *Var* represents the variance.

The ecological detector can then be applied to discern whether there is a significant difference between two factors' influence on the spatial distribution of AWF, tested with the F statistic:

$$F = \frac{N_{X1}(N_{X2} - 1)SSW_{X1}}{N_{X2}(N_{X1} - 1)SSW_{X2}} \quad (9)$$

$$SSW_{X1} = \sum_{h=1}^{L1} N_h \sigma_h^2 , \quad SSW_{X2} = \sum_{h=1}^{L2} N_h \sigma_h^2 \quad (10)$$

where N_{X1} and N_{X2} denote the size of the samples of the two factors *X*1 and *X*2,

respectively; SSW_{X1} and SSW_{X2} are the sum of squares in the subregions generated by factor strata *X1* and *X2*, respectively.

Geographical detector was implemented in MS Excel software, where it can be run with a maximum of 32,767 rows of data. Hence, it was necessary to first convert the spatial data into point data. To select sufficient representative point data for the entire irregular afforestation area, we generated 300-m × 300-m fishing nets in ArcGIS software, to finally obtain 30,799 random sample points (Fig. A.3). The AWF of these sampling points and its data on related factors were extracted from the attribute table, upon which the geographical detector analysis was conducted.

3 Results

3.1 Spatial distribution of afforestation across the desert regions of northern China

According to the NDVI trend analysis for the 2003–2017 period, the NDVI increased significantly in most areas but was mainly distributed in the east and south of desert regions, indicating that the ecological environment has improved there especially (Fig. 2c). Within these NDVI-increased land areas, their forest cover was designated as afforestation that is mainly distributed in the southeast and south (Fig. 3). The total afforestation area increased by 73,764.31 km^2 from 2003 to 2017, accounting for 2.42% of the total study area (Table B.1.). At the desert areas scale, IMGW had the largest afforestation with an area of 35,962.61 km^2, accounting for the 48.75% of the total afforestation area. In the IMGW, the afforestation was mainly distributed in the east of this particular region, where *bash* had the largest afforestation area at 12,120.63 km^2. The TRHR's afforestation area is second only to IMGW, and mainly concentrated in the south of TRHR, accounting for 27.89% of the total afforestation area. In the ARNC, afforestation was found distributed primarily in *zhgr* and *hxzl*, respectively accounting for 38.65% and 29.91% of the entire

afforestation area in the ARNC.

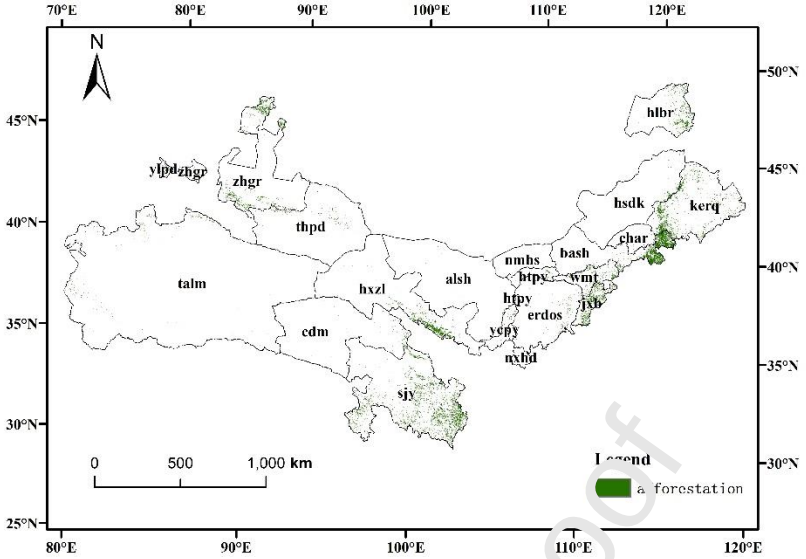

Fig. 3. Afforestation in desert region of northern China (2003–2017).

3.2 Afforestation WF

During the 2003–2017 study period, the average AWF was 8.41 m^3/gC across all desert regions of northern China. The AWF increased from east to west, indicative of spatial heterogeneity (Fig. 4). At the desert areas scale, TRHR had the highest average AWF, followed by ARNC and IVGW. At the subregional scale, *alsh*, *ycpy*, *talm*, and *htpy* had the highest-ranked average values of AWF, these being 18.51 m^3/gC, 13.03 m^3/gC, 12.53 m^3/gC, and 11.73 m^3/gC, respectively.

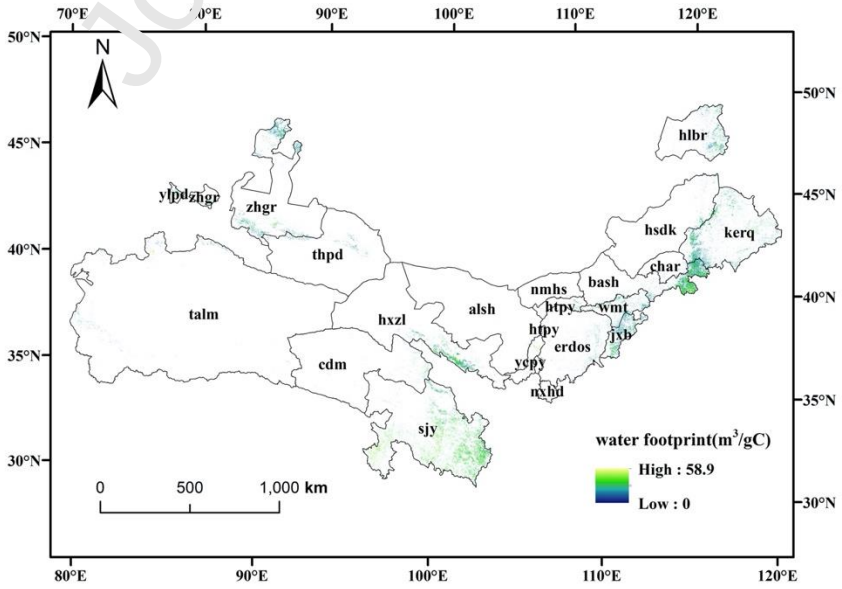

Fig. 4. Spatial distribution of the average AWF (m3/gC).

Concerning the WF's composition, the blue WF was higher than the green WF, on average, largely due to the limited rainfall across northern China. Nonetheless, there were obvious distinctions among the desert areas. The TRHR had the highest proportion of green WF, followed by IMGW and ARNC. In the subregions of IMGW, the difference between the green and blue WF was relatively small in *wmt*, *char*, and *jxb*, whereas *erdos* had as higher green WF than blue WF. In the ARNC, the blue WF exceeded the green WF in most subregions except *cdm* and *thpd* (Fig. 5).

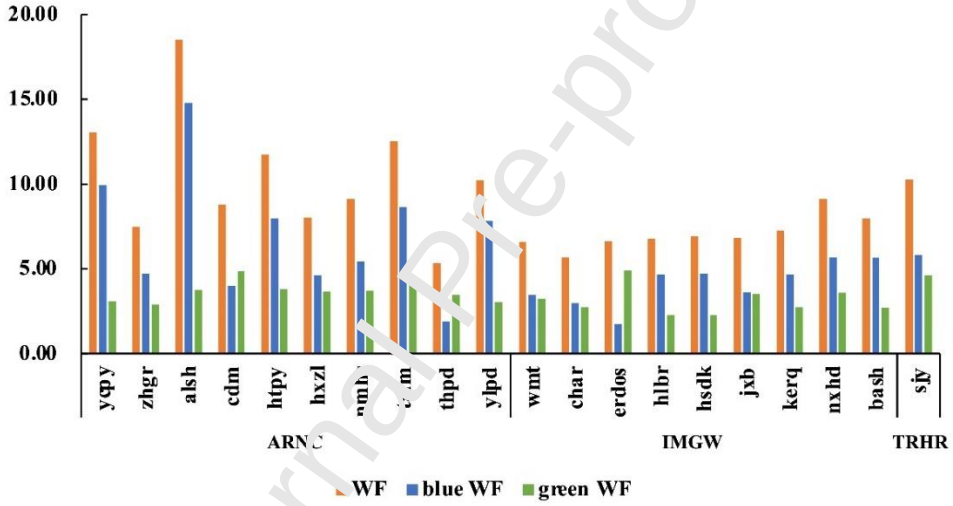

Fig. 5 The average afforestation WF of the subregions (m^3/gC).

3.3 Influences of natural and human factors on AWF

3.3.1 Effects of the 12 factors on AWF

The respective impact (q-values) of the 12 factors upon AWF and its components (i.e., blue and green WF) were obtained from the factor detector (Table 3). Among all factors, potential evapotranspiration had the largest influence, explaining 20.4% of the variation in AWF. By contrast, the total contribution from GDP, population, and the distance from road was just 2%, implying that human factors had less impact of an

impact on AWF. For the blue and green WF, the main factors driving each were temperature and elevation, respectively. At the desert areas scale, the main factors affecting the AWF differed, for which the top three factors are presented in Figure 6. In the ARNC, temperature, potential evapotranspiration, and soil type were the major factors explaining the AWF and blue WF (sorted in descending order of q-value). In the IMGW, the AWF was mainly contributed to by soil type, geomorphic type, and temperature. In the TRHR, it was elevation, temperature, and potential evapotranspiration that chiefly influenced the AWF.

In summary, natural factors had far greater impacts on the AWF than did human factors, especially among the desert areas. However, at the subregional scale, human factors could contribute more to explaining the patterns of AWF. For example, in *htpy* and *thpd*, distance from road and county influenced the AWF and also its green and blue WF.

Table 3 q-values of different factors on AWF, Blue WF and Green WF

	pet	prec	temp	ws	ir	dem	gmt	soil	gdp	pop	dfr	dfc
AWF	0.204	0.164	0.186	0.0[illegible]	0.137	0.113	0.047	0.167	0.003	0.006	0.013	0.000[#]
Blue WF	0.114	0.092	0.150	0.0[illegible]	0.054	0.011	0.048	0.123	0.002	0.001*	0.002	0.003
Green WF	0.390	0.162	0.[illegible]28	0.029	0.207	0.421	0.023	0.302	0.002	0.026	0.038	0.006

Note: * denotes a q-value found significant at the 0.05 level ($p < 0.05$); [#] denotes a q-value is significant at the 0.1 level ($p < 0.1$). Other values without any superscript symbols denotes a q-value is significant at the 0.01 level ($p < 0.01$).

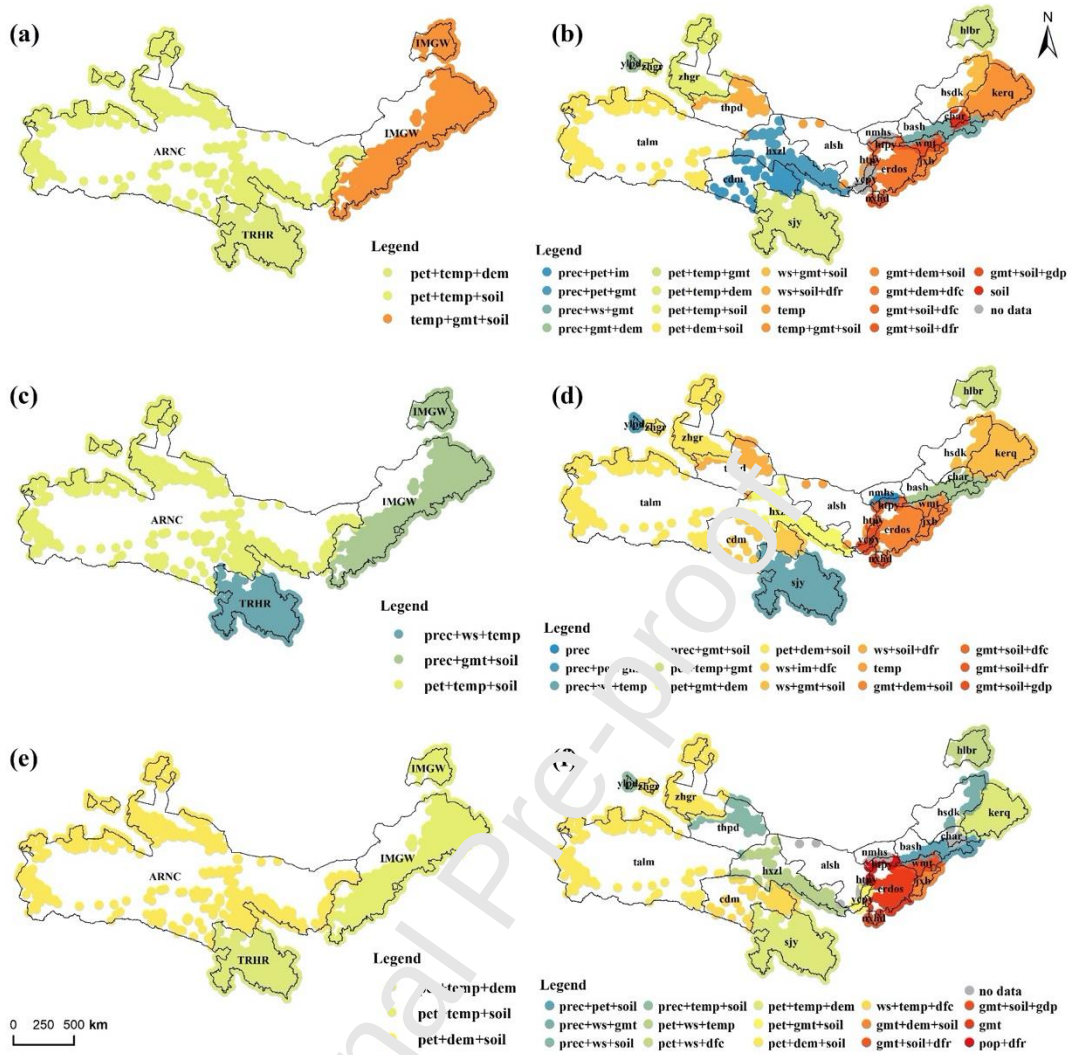

Fig. 6. The main factors affecting the WF in the desert regions and subregions. (a), (b) Main factors of WF. (c), (d) Main factors of blue WF. (e), (f) Main factors of green WF.

3.3.2 Interaction between factors

The interaction detector analyzed the 12 factors' influence on AWF across the whole afforestation area (Fig. B.2). Since the q-value of each pair is evidently larger than that either single factor, the explanatory power of a single factor can be strengthened by its interaction with another factor. The vast majority (80.3%) of interaction effects were a non-linearly enhanced form. The rest (19.7%) took the form of bivariate enhanced, which mainly occurred when potential evapotranspiration,

precipitation, and temperature interacted with other factors. For the blue WF, the interactions were mainly non-linearly enhanced, this accounting for 89.4% of all cases. The interaction between soil type and climate factors had a higher impact on the blue WF than the green WF. For the green WF, the proportion of bivariate enhanced interactive effects reached 39.4%. The interactions between the elevation, soil type and climate factors exerted a greater impact on the green than blue WF. For the desert areas and subregions, the analysis also resulted in the q-value of each pair of factors being higher than that of their single factors. Potential evapotranspiration, temperature, soil types, and elevation were the principal influencing factors, the interactions between them and other factors surpassed those of other factor interactions.

3.3.3 Effect of factors' different grades

By using the risk detector, the AWF in the different grades of all 12 factors were obtained (Fig. 7). Those grades with the highest AWF can be recognized as the leading grade for each factor. The impact of the climate factors' different grades on the average WF was clearly not uniform. Taking potential evapotranspiration and precipitation as examples, the AWF increased with more potential evapotranspiration, but as precipitation increased, the AWF tended to decrease as well. With increasing elevation, the AWF also tended to increasing, and the grade-1 (plain) geomorphic type and the grade-9 (saline soil) soil type each had a higher AWF. With respect to the human factors, the AWF for their different grades were similar, though regions with a lower GDP and population may have higher AWF. For distance from county, its grade-1, -2, and -3 had no significant impacts on the AWF. The average green and blue WF also differed starkly among the grades of all 12 factors (Fig. B.3). The blue WF increased with the more potential evapotranspiration and a higher temperature yet decreased with more precipitation and a greater wind speed. By contrast, the green

WF did not change significantly with variation in any climate factor. For the human factors, the different grades of these factors also had negligible or little effect on the blue and green WF.

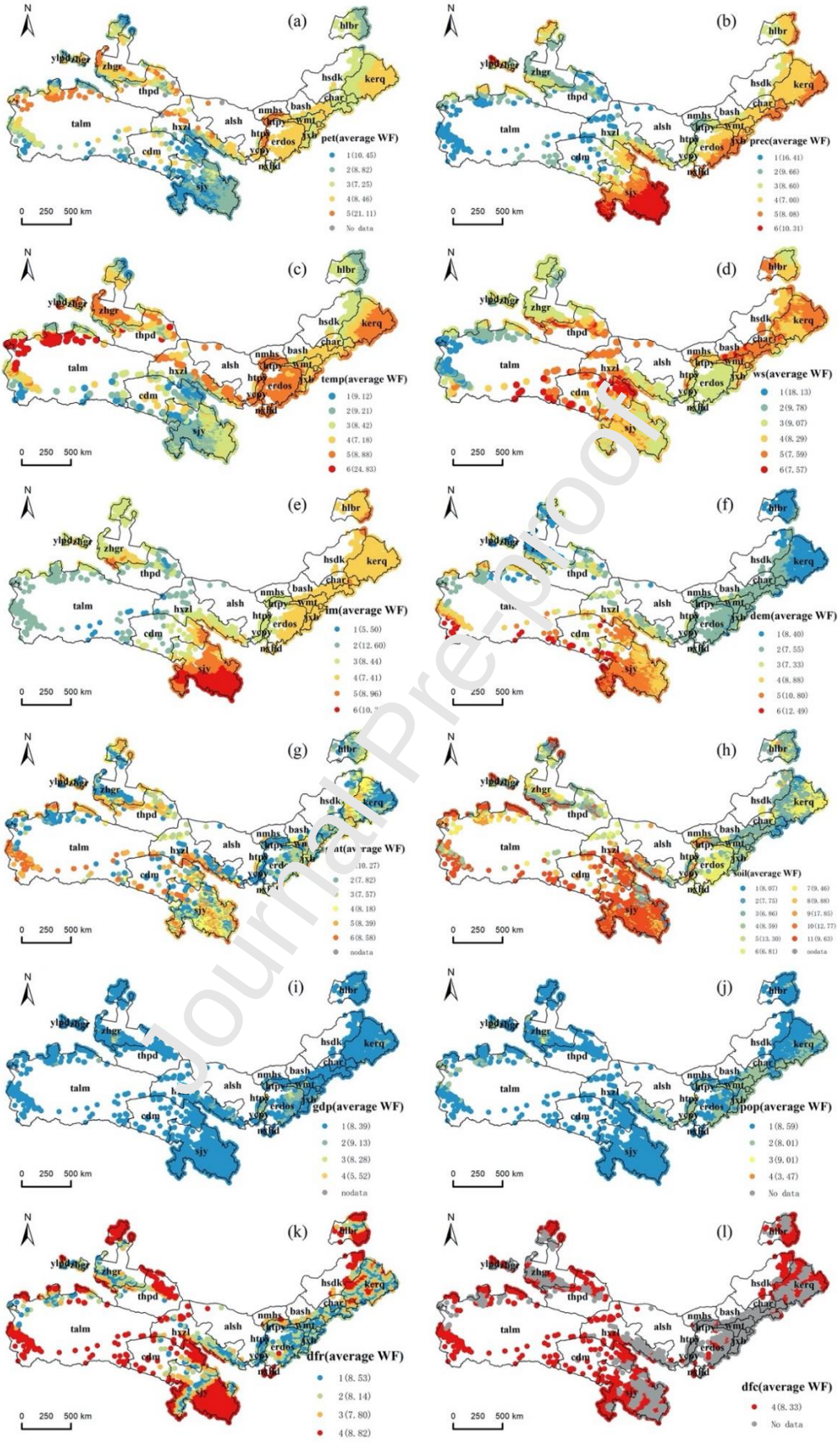

Fig. 7. The average AWF in the different grades of 12 factors (m^3/gC).

3.3.4 Significant differences between the factors

The differential impact of paired factors upon the AWF was determined using an ecological detector analysis. These results showed significant differences in impact between most paired factors, but not so among the four human factors (Fig. B.4). Likewise, no significant differences were detected between soil type and precipitation, or between wind speed and geomorphic type. With respect to the blue WF, non-significant differences between elevation and human factors, wind speed, and moisture index were found. For the green WF, the difference in impacts between most of the paired factors were statistically significant, yet not so between wind speed, population, geomorphic types, and distance from road, as well as GDP and distance from county, temperature, and moisture index. Overall, natural factors had the stronger effects than did human factors on WF, and also the green and blue WF.

4 Discussion

4.1 Identification of afforestation

The afforestation coverage and trends identified in this study are consistent with the distribution characteristics of China's afforestation project and work by Zhang et al. (2016) and Yin et al. (2018), which revealed that large-scale ecological construction has achieved certain progress since 2002. Accurately quantifying afforestation is important for the calculation and analysis of AWF. Here, texture classification was chosen to distinguish land cover in this study and its accuracy was 80%, in line with its superior performance at separating different land types from remotely sensed imagery (Murray et al., 2010). Due to the poor identification of some recent sites of afforestation or with shrub vegetation, the actual land area under afforestation may have been slightly underestimated. In a future study, we plan to extract the multi-temporal afforestation and analyze afforestation at different temporal

and spatial scales.

4.2 Afforestation water footprint (AWF)

Referring to the calculation of the WF for crop plants, here we used NPP as an indicator of afforestation production to calculate the AWF in northern China. The results showed the distribution of AWF was spatially dependent, in that it gradually increased going from east to west. Meanwhile, most regions featured a higher proportion of blue than green WF, thus indicating that afforestation consumed more groundwater. Similarly, Lu et al. (2018) also found that under varying assumptions, afforestation would cause the groundwater table to decline in arid and semi-arid regions in northern China. The respective proportion of blue and green WF could reveal the water use efficiency to some extent (Lu et al., 2016). A higher proportion of green WF suggests water consumption of precipitation mainly and this entails a higher water use efficiency and lower water opportunity cost. Earlier, Zeng et al (2012) reported that in arid and semi-arid regions, the blue WF proportion of crop production exceeded China's average amount. Therefore, in arid and semi-arid regions, afforestation could put potential pressure on local water resources. In devising or implementing further ecological restoration practices, selecting native tree species with high water-use efficiency is important to utilize the groundwater resource more efficiently and sustainably.

4.3 Driving forces of AWF

Our detector analysis results showed that at different scales the explanatory power of natural and human factors for the AWF was disparate. At the whole study area scale, climate factors predominately impact the AWF, namely potential evapotranspiration, precipitation, and temperature. Potential evapotranspiration can be regarded as a comprehensive indicator of climatic conditions, on that has been shown

to be influenced by temperature and vapor pressure deficit but also able to affect vegetation growth to some extent (You et al., 2019). Notably, with more precipitation, the blue WF decreased and the water use efficiency of afforestation was improved. Although a moderate increase in temperature can promote vegetation growth, too much warming can accelerate evaporation sufficiently to limit vegetation growth (Li et al., 2018). At the desert areas scale, the impact of elevation, soil type, and geomorphic type on AWF were all increased. Among them, soil type played an important role in vegetation growth, a result consistent with the findings of Meng et al. (2020). A previous study also indicated that when the precipitation is the leading factor, the type of soil will strongly determine vegetation growth and rainwater reuse (Otgonbayar et al., 2017). When compared with natural factors, the human factors we investigated had much less of an influence on AWF across the whole study area. Yet at the subregional scale, human factors can markedly impact the AWF; for example, in the *thpd*, distance from road had the highest q-value, suggesting that the AWF there was shaped by human activities. Additionally, in the regions with similar climatic characteristics, the influence from other factors may increase: for instance, in *nxhd*, the climate factors only include two grades, and the main factors affecting AWF include soil type, geomorphic type and distance from road without climate factors.

We found that the interactions between influencing factors often enhanced their effects not only upon the AWF but also the blue and green WF. Importantly, the explanatory power of interacting factors tends to increase at smaller spatial scales of inquiry. Although individually the human factors had less of an impact on the AWF in general, their explanatory power may be enhanced when through interaction with natural factors. Recent research suggests the interactive influence of natural factors on NDVI happens through a bivariate or nonlinear enhancement (Peng et al., 2019). We

might expect that, under particular climatic conditions, one or more human factors would strengthen the impact on vegetation (Tong et al., 2020).

In summary, based on the spatial stratification of impacting factors, the analysis of driving forces acting on AWF could provide a more robust reference that could inform or guide policymakers seeking appropriate measures for effectively implementing ecological restoration. Specifically, choosing a suitable region with favorable soil and geomorphic types for the afforestation's implementation is crucial. Additionally, water-saving technologies such as drip irrigation should be adopted to conserve water, and native and drought-resistant tree species ought to be selected for planting to improve the recruitment and survival of saplings. Furthermore, adjusting the planting density in afforestation can help reduce competition between trees for water resources. Above all, the carrying capacity of water resources should be fully considered when implementing any afforestation project in arid and semi-arid regions.

5 Conclusions

Based on the Landsat datasets coupled with meteorological, soil type, socio-economic as well as other data, the afforestation area, WF, and the factors influencing the AWF were analyzed across desert regions of northern China, from 2003–2017. On the whole, the afforestation had increased by 73,764.31 km^2 over this time period, and the AWF increased going from east to west. In this study, the impacts of different factors on the AWF were quantitatively analyzed by the geographical detector method. We found that potential evapotranspiration, temperature, soil types, and precipitation were the dominant factors influencing afforestation's WF across the whole study area. However, the major contributing factors differed among different desert areas and subregions. The interaction between each pair of factors exhibited bivariate enhancement or nonlinear enhancement, indicating that the interactions

between different factors had higher impact than that of single factors. Notably, the risk detector results revealed a range of different factors that would lead to higher afforestation WFs. Therefore, policymakers should consider local natural conditions, such as the annual precipitation, temperature, and soil types along with socio-economic factors, when carrying out afforestation. Looking ahead, we plan to analyze afforestation's WF at multiple temporal scales, to further inform the sustainability of ecological restoration efforts, especially in arid and semi-arid areas.

Acknowledgements: This research is jointly supported by National Natural Science Foundation of China (41971253) and National Key Research and Development Program of China (2017YFC0506704).

Appendix A. Study area and data description

Appendix A.1. The names of the subregions in the study area.

Abbreviation	Name	Abbreviation	Name
hlbr	Hulun Buir	*cdm*	Chaidamu
horq	Horqin	*alsh*	Alashan plateau
hsdk	Hunshandake	*htpy*	Hetao plain
char	Chahar	*hxzl*	Hexi Corridor
bash	Bashang	*nmhs*	Houshan region in Inner Mongolia
wmt	Wumeng Qianshan and Tumote plain	*talm*	Tarim basin
jxb	Northwest area of Shanxi Province	*thpd*	Turpan Hami basin
erdos	Erdos	*ycpy*	Yinchuan plain
nxhd	Ningxia Hedong	*ylpd*	Yili basin
trhr	Three-River Headwaters	*zhgr*	Zhungeer basin

Appendix A.2. Stratification of the 12 influencing factors.

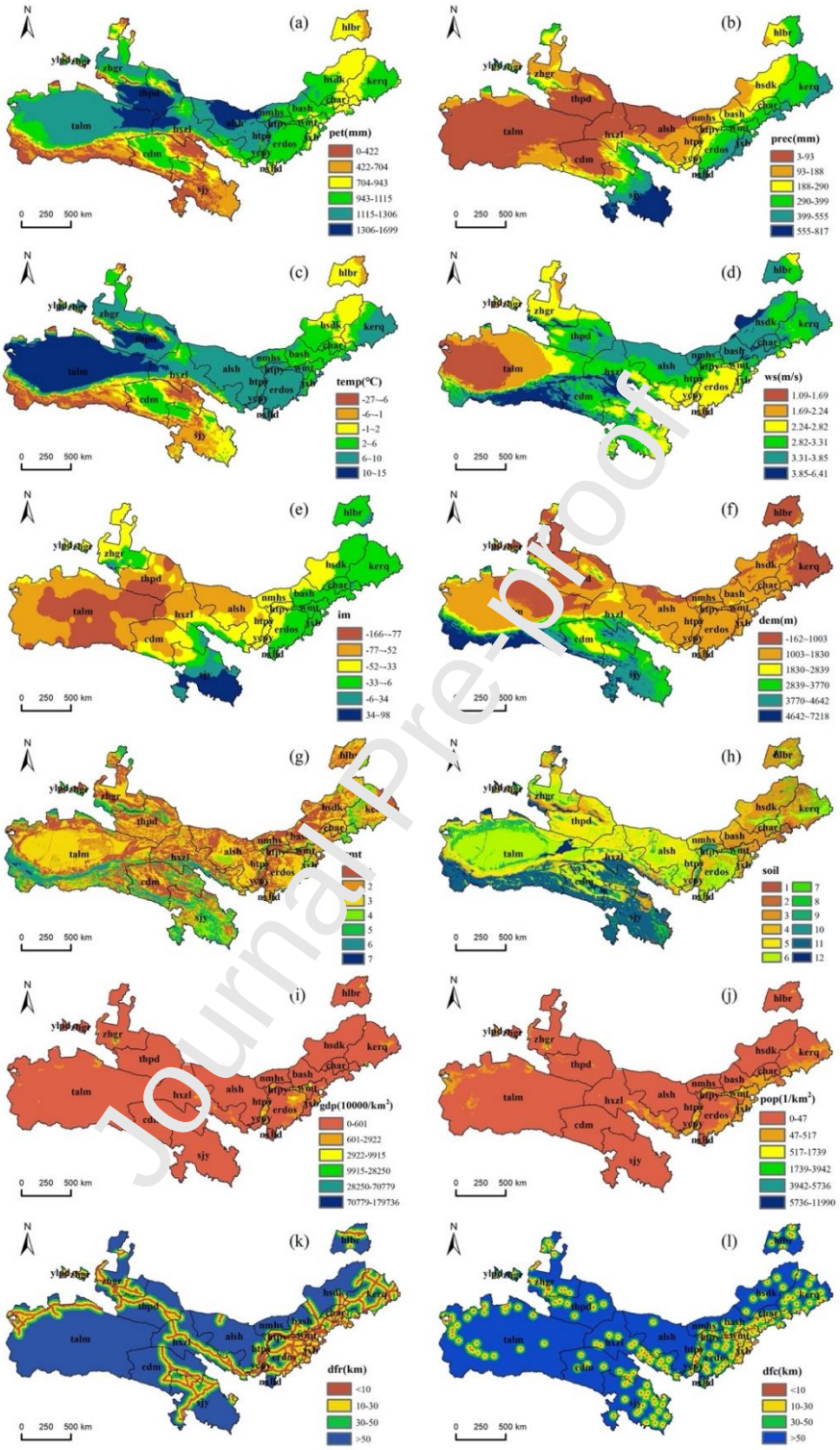

The serial numbers in the legend of soil type denote the following: (1) leached soils, (2) semi-leached soils, (3) pedocal, (4) aridisols, (5) desert soil, (6) primary soils, (7) semi-hydrated soils, (8) water-formed soils, (9) saline soil, (10) water-formed soils, (11) ferro alumina soils, and

(12) rocks and other. The serial numbers in the legend of gmt correspond to (1) plain, (2) terraces, (3) hill, (4) small undulating mountains, (5) middle undulating mountains, (6) large undulating mountains, and (7) extremely undulating mountains.

Appendix A.3. The spatial distribution of sample points.

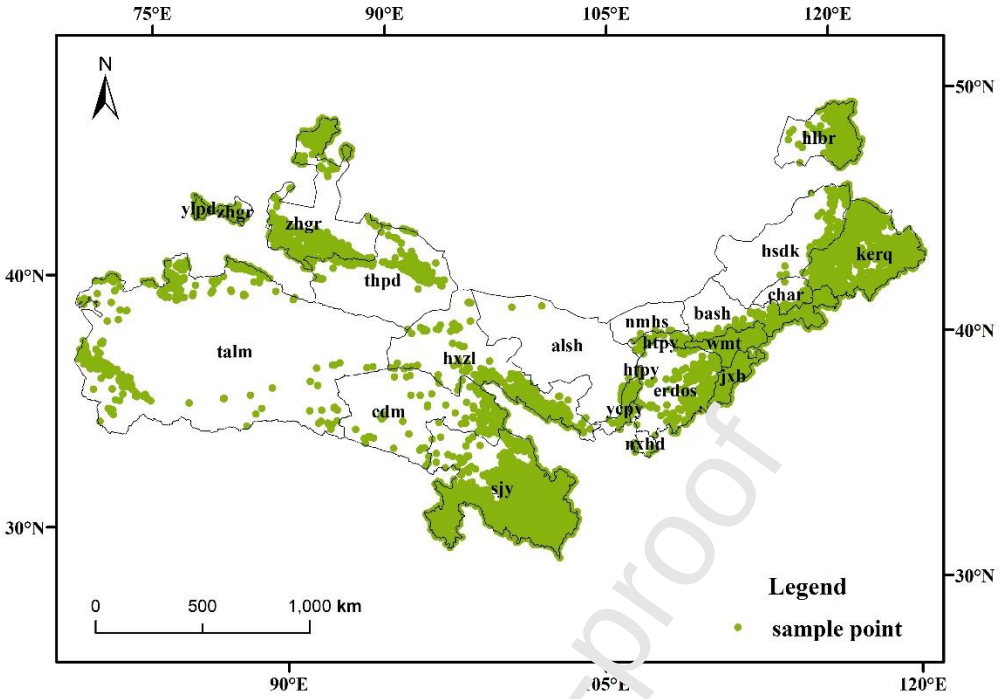

Appendix. B Results supplementary

Appendix B.1. The land under afforestation in the different subregions.

Desert areas	Subregion	Area (km^2)
ARNC	*ycpy*	573.53
	zhgr	6659.83
	alsh	133.72
	cdm	723.18
	htpy	389.52
	hxzl	5154.02
	nmhs	35.53
	talm	1694.35
	tlpa	1194.68
	ylpd	671.42
IMGW	*hlbr*	3485.98
	kerq	10157.17
	hsdk	966.89
	char	211.16
	bash	12120.63
	wmt	2596.81
	jxb	4949.77
	erdos	1344.95
	nxhd	129.25
TRHR	*sjy*	20571.92
Total area		**73764.31**

Appendix B.2. Interactions detected between different factors on the afforestation WF (a), blue WF (b), and green WF (c).

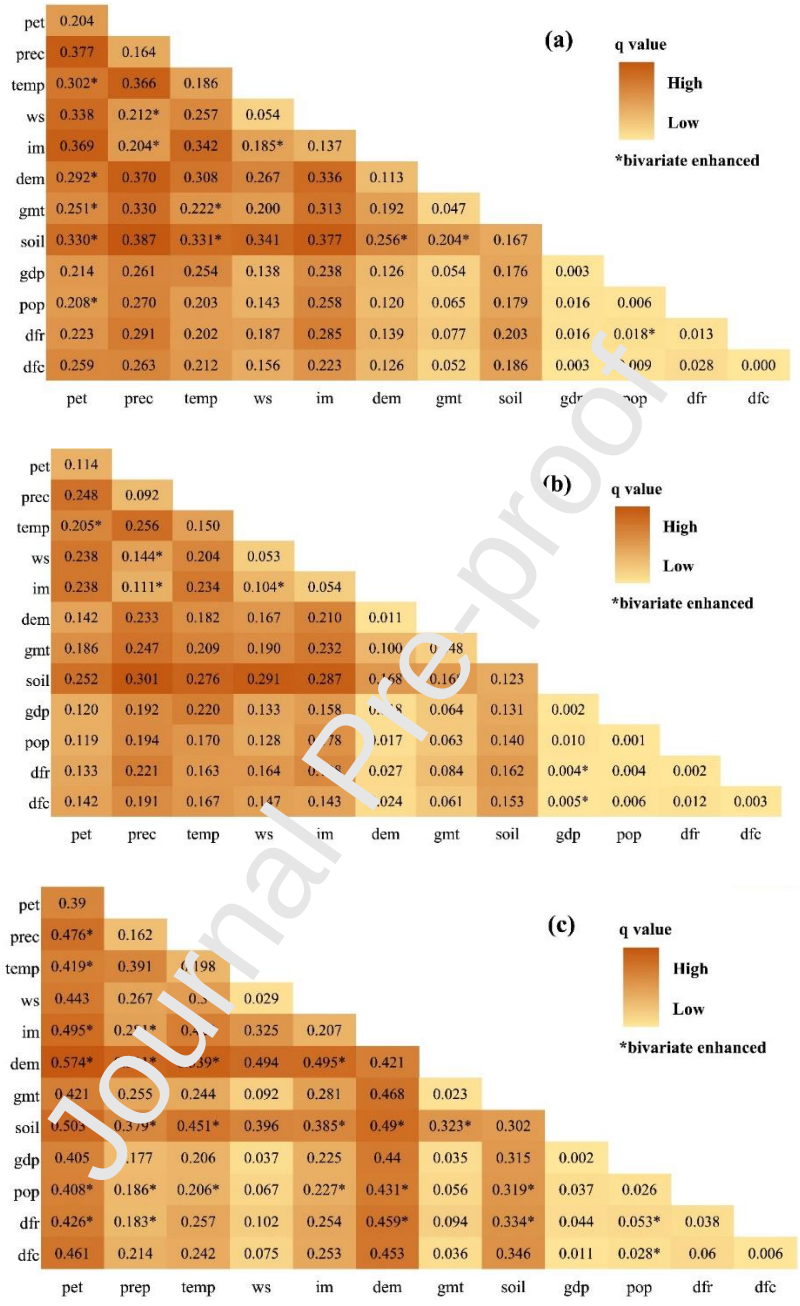

* denotes an interactive relationship that was enhanced, bivariate; otherwise, the interactive relationship is nonlinearly enhanced.

Appendix B.3. Factor grades and their corresponding average blue and green WF (m^3/gC).

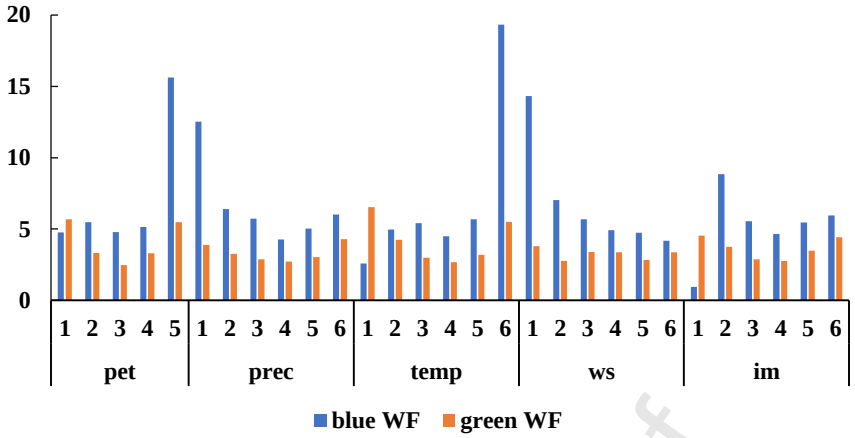

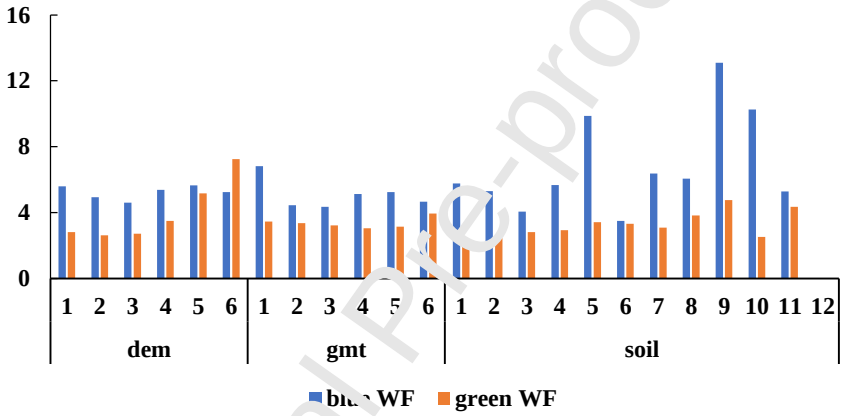

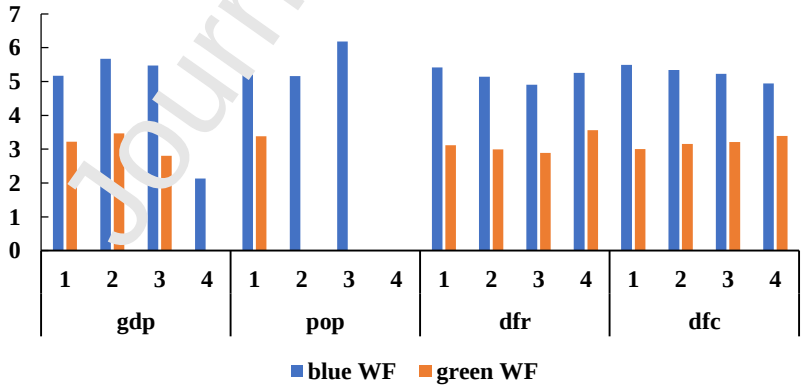

Appendix B.4. The ecological detector results: (a) WF, (b) blue WF, (c) green WF.

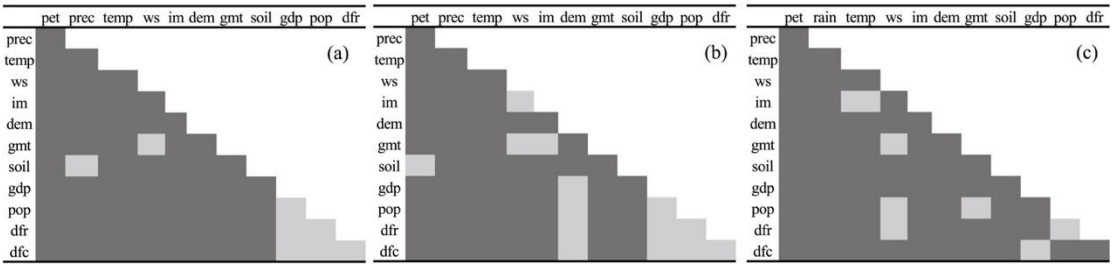

Dark gray denotes ‘Y’, the light gray denotes ‘N’, respectively referring to a Yes or No significant difference between the given two factors.

References

Amiraslani, F., Dragovich, D., 2011. Combating desertification in Iran over the last 50 years: an overview of changing approaches. Journal of environmental management 92, 1-13.

An, W.M., Li, Z.S., Wang, S., Wu, X., Lu, Y.H., Liu, G.H., Fu, B.J., 2017. Exploring the effects of the "Grain for Green" program on the differences in soil water in the semi-arid Loess Plateau of China. Ecological Engineering 107, 144-151.

Barry, L.E., Yao, R.T., Harrison, D.R., Paragahawewa, U.H., Pannell, D.J., 2014. Enhancing ecosystem services through afforestation: How policy can help. Land Use Policy 39, 135-145.

Bastin, J.F., Finegold, Y., Garcia, C., Mollicone, D., Rezende, M., Routh, D., Zohner, C.M., Crowther, T.W., 2019. The global tree restoration potential. Science 365, 76-79.

Beck, P.S.A., Atzberger, C., Høgda, K.A., Johansen, B., Skidmore, A.K., 2006. Improved monitoring of vegetation dynamics at very high latitudes: A new method using MODIS NDVI. Remote Sensing of Environment 99, 321-334.

Bocchiola, D., Nana, E., Soncini, A., 2013. Impact of climate change scenarios on crop yield and water footprint of maize in the Po valley of Italy. Agricultural Water Management 116, 50-61.

Cao, J.J., Tian, H., Adamowski, J.F., Zhang, X.F., Cao, Z.J., 2018. Influences of afforestation policies on soil moisture content in China's arid and semi-arid regions. Land Use Policy 75, 449-458.

Cao, S.X., Zhang, J.Z., 2015. Political risks arising from the impacts of large-scale afforestation on water resources of the Tibetan Plateau. Gondwana Research 28, 898-903.

Cao, S.X., Zhang, J.Z., Chen, L., Zhao, T.Y., 2016. Ecosystem water imbalances created during ecological restoration by afforestation in China, and lessons for other developing countries. Journal of environmental management 183, 843-849.

Chen, C., Park, T., Wang, X.H., Piao, S.L., Xu, B.D., Chaturvedi, R.K., Fuchs, R., Brovkin, V., Ciais, P., Fensholt, R., Tommervik, H., Bala, G., Zhu, Z.C., Nemani, R.R., Myneni, R.B., 2019. China and India lead in greening of the world through land-use management. Nature sustainability 2, 122-129.

Chen, L.F., He, Z.B., Zhu, X., Du, J., Yang, J.J., Li, J., 2016. Impacts of afforestation on plant diversity, soil properties, and soil organic carbon storage in a semi-arid grassland of northwestern China. Catena 147, 300-307.

Chouchane, H., Hoekstra, A.Y., Krol, M.S., Mekonnen, M.M., 2015. The water footprint of Tunisia from an economic perspective. Ecological Indicators 52, 311-319.

D'Ambrosio, E., De Girolamo, A.M., Rulli, M.C., 2018. Assessing sustainability of agriculture through water footprint analysis and in-stream monitoring activities. Journal of Cleaner Production 200, 454-470.

Duan, Q.W., Tan, M.H., 2020. Using a geographical detector to identify the key factors that influence urban forest spatial differences within China. Urban Forestry & Urban Greening 49, 126623.

Ellison, D., Ifejika Speranza, C., 2020. From blue to green water and back again: Promoting tree, shrub and forest-based landscape resilience in the Sahel. Science of the total environment 739, 140002.

Fan, J.L., Wang, J.D., Zhang, X., Kong, L.S., Song, Q.Y., 2019. Exploring the changes and driving forces of water footprints in China from 2002 to 2012: A perspective of final demand. Science of the total environment 650, 1101-1111.

FAO, 2010. Food and Agriculture Organization of the United Nations: land and water development division. CROPWAT Model. FAO, Rome, Italy

Hoekstra, A.Y., 2003. Virtual Water Trade: Proceedings of the International Expert Meeting on Virtual Water Trade. Value of Water Research Report Series No. 12. UNESCOIHE, Delft, The Netherlands.

Hoekstra, A.Y., Chapagain, A.K., Aldaya, H.M., Mekonnen, H.M., 2011. The Water Footprint Assessment Manual: Setting the Global Standard. Earthscan, London

Hua, W.J., Chen, H.S., Zhou, L.M., Xie, Z.H., Qin, M.H., Li, X., Ma, H.D., Huang, Q.H., Sun, S.L., 2017. Observational Quantification of Climatic and Human Influences on Vegetation Greening in China. Remote Sensing 9, 425.

Huang, J.X., Wang, J.F., Bo, Y.C., Xu, C.D., Yu, M.G., Huang, D.C., 2014. Identification of Health Risks of Hand, Foot and Mouth Disease in China Using the Geographical Detector Technique. International Journal of Environmental Research & Public Health 11, 3407-3423.

IPBES. 2018. In L. Montanarella, R. Scholes, & A. Brainich (Eds.), The IPBES assessment report on land degradation and restoration. Bonn, Germany: Secretariat of the Intergovernmental Science- Policy Platform on Biodiversity and Ecosystem Services. Retrieved from https://www.ipbes.net/

Kirschbaum, M.U.F., Whitehead, D., Dean, S.M., Beets, P.N., Shepherd, J.D., Ausseil, A.G.E., 2011. Implications of albedo changes following afforestation on the benefits of forests as carbon sinks. Biogeosciences 8, 8563-8589.

Li, D.J., Xu, D.Y., Wang, Z.Y., You, X.G., Zhang, X.Y., Song, A.L., 2018. The dynamics of sand-stabilization services in Inner Mongolia, China from 1981 to 2010 and its relationship with climate change and human activities. Ecological Indicators 88, 351-360.

Liang, P., Yang, X., 2016. Landscape spatial patterns in the Maowusu (Mu Us) Sandy Land, northern China and their impact factors. CATENA 145, 321-333.

Liu, B.J., Zhang, L., Lu, F., Deng, L., Zhao, H., Luo, Y.J., Liu, X.P., Zhang, K.R., Wang, X.K., Liu, W.W., Wang, X.Y., Yuan, Y.F., 2019. Greenhouse gas emissions and net carbon sequestration of the Beijing-Tianjin Sand Source Control Project in China. Journal of Cleaner Production 225, 163-172.

Liu, Y., Miao, H.T., Huang, Z., Cui, Z., He, H.H., Zheng, J.Y., Han, F.P., Chang, X.F., Wu, G.L., 2018. Soil water depletion patterns of artificial forest species and ages on the Loess Plateau (China). Forest Ecology and Management 417, 137-143.

Lovarelli, D., Bacenetti, J., Fiala, M., 2016. Water Footprint of crop productions: A review. Science of the total environment 548-549, 236-251.

Lu, C.X., Zhao, T.Y., Shi, X.L., Cao, Y., 2018. Ecological restoration by afforestation may increase groundwater depth and create potentially large ecological and water opportunity costs in arid and semiarid China. Journal of Cleaner Production 176, 1213-1222.

Lu, Y., Zhang, X.Y., Chen, S.Y., Shao, L.W., Sun, H.Y., 2016. Changes in water use efficiency and water footprint in grain production over the past 35 years: a case study in the North China Plain. Journal of Cleaner Production 116, 71-79.

Ma, H., Lv, Y., Li, H.X., 2013. Complexity of ecological restoration in China. Ecological Engineering 52, 75-78.

Ma, W.J., Opp, C., Yang, D.W., 2020. Spatiotemporal supply-demand characteristics and economic benefits of crops water footprint in semi-arid region. Science of The Total Environment 738, 139502.

Meng, X.Y., Gao, X., Li, S.Y., Lei, J.Q., 2020. Spatial and Temporal Characteristics of Vegetation NDVI Changes and the Driving Forces in Mongolia during 1982–

2015. Remote Sensing 12, 603.

Murray, H., Lucieer, A., Williams, R., 2010. Texture-based classification of sub-Antarctic vegetation communities on Heard Island. International Journal of Applied Earth Observation & Geoinformation 12, 138-149.

Novoa, V., Ahumada-Rudolph, R., Rojas, O., Munizaga, J., Sáez, K., Arumí, J.L., 2019. Sustainability assessment of the agricultural water footprint in the Cachapoal River basin, Chile. Ecological Indicators 98, 19-28.

Otgonbayar, M., Atzberger, C., Chambers, J., Amarsaikhan, D., Tsogtbayar, J., 2017. Land Suitability Evaluation for Agricultural Cropland in Mongolia Using the Spatial MCDM Method and AHP Based GIS. Journal of Geoscience and Environment Protection 05, 238-263.

Peng, W.F., Kuang, T.T., Tao, S., 2019. Quantifying influences of natural factors on vegetation NDVI changes based on geographical detector in Sichuan, western China. Journal of Cleaner Production 233, 353-367.

Prabakaran, C., Singh, C.P., Panigrahy, S., Parihar, J.S., 2013. Retrieval of forest phenological parameters from remote sensing-based NDVI time-series data. Current ence 105, 785.

Schwarzel, K., Zhang, L., Montanarella, L., Wang, Y., Sun, G., 2020. How afforestation affects the water cycle in drylands: A process-based comparative analysis. Glob Chang Biol 26, 944-959.

Tie, Q., Hu, H.C., Tian, F.Q., Holbrook, N.M., 2018. Comparing different methods for determining forest evapotranspiration and its components at multiple temporal scales. Science of the total environment 633, 12-29.

Tong, Y.J., Wen Y.J., Zhang, C. 2020. Spatiotemporal Variation of NDVI and Its Influence Factors in Shaanxi Province During 2003-3017. Bulletin of Soil and

Water Conservation 40(3), 155-162. (In Chinese)

UNCCD. 2017. The Global Land Outlook, 1st ed.; United Nations Convention to Combat Desertification: Bonn, Germany.

Wahba, S.M., 2021. Understanding internal water footprint inequality of the Egyptian households based on different income and lifestyles. Journal of Cleaner Production 288, 125112.

Wang, X.M., Zhang, C.X., Hasi, E., Dong, Z.B., 2010a. Has the Three Norths Forest Shelterbelt Program solved the desertification and dust storm problems in arid and semiarid China? Journal of Arid Environments 74, 13-22.

Wang, J.F., Li, X.H., Christakos, G., Liao, Y.L., Zhang, T., Gu, X., Zheng, X.Y., 2010b. Geographical Detectors-Based Health Risk Assessment and its Application in the Neural Tube Defects Study of the Heshun Region, China. International Journal of Geographical Information Science 24, 107-127.

Wang, J.F., Xu, C.D., 2017. Geodetector: principle and prospective. Acta Geograph. Sin. 1,116–134. (In Chinese)

West, T.A.P., Monge, J.J., Downing, L., Wakelin, S.J., Gibbs, H.K., 2020. Promotion of afforestation in New Zealand's marginal agricultural lands through payments for environmental services. Ecosystem Services 46, 101212.

Wu, W.Q., Zhang, M., Ding, Y.T., 2020. Exploring the effect of economic and environment factors on PM2.5 concentration: A case study of the Beijing-Tianjin-Hebei region. Journal of environmental management 268, 110703.

Xiao, Y., Xiao, Q., Sun, X.F., 2020. Ecological Risks Arising from the Impact of Large-scale Afforestation on the Regional Water Supply Balance in Southwest China. Scientific reports 10, 4150.

Xie, S.D., Mo, X., Hu, S., Liu, S.X., 2020. Contributions of climate change, elevated atmospheric CO2 and human activities to ET and GPP trends in the Three-North Region of China. Agricultural and Forest Meteorology 295, 108183.

Xu, D.Y., Li, D.J., 2020. Variation of wind erosion and its response to ecological programs in northern China in the period 1981–2015. Land Use Policy 99, 104871.

Yang, Q.C., Tian, H.Q., Li, X., Tao, B., Ren, W., Chen, G.S., Lu, C.Q., Yang, J., Pan, S.F., Banger, K., Zhang, B.W., 2015. Spatiotemporal patterns of evapotranspiration along the North American east coast as influenced by multiple environmental changes. Ecohydrology 8, 714-725.

Yin, H., Pflugmacher, D., Li, A., Li Z.G., Hostert, P., 2018. Land use and land cover change in Inner Mongolia - understanding the effects of China's re-vegetation programs, Remote Sensing of Environment. 918-930.

You, G.Y., Arain, M.A., Wang, S.S., Lin, N.F., Gao, J.X., 2019. Trends of actual and potential evapotranspiration based on Bouchet's complementary concept in a cold and arid steppe site of Northeastern Asia. Agricultural and Forest Meteorology 279, 107684.

Yuan, W.P., Li, X.L., Liang, S.L., Cui, X.F., Dong, W.J., Liu, S.G., Xia, J.Z., Chen, Y., Liu, D., Zhu, W.Q., 2014. Characterization of locations and extents of afforestation from the Grain for Green Project in China. Remote Sensing Letters 5, 221-229.

Zeng, Z., Liu, J., Koeneman, P.H., Zarate, E., Hoekstra, A.Y., 2012. Assessing Water Footprint at River Basin Level: A Case Study for the Heihe River Basin in Northwest China. Hydrology and Earth System sciences 16, 2771-2781.

Zhang, Y., Peng, C.H., Li, W.Z., Tian, L.X., Zhu, Q.A., Chen, H., Fang, X.Q., Zhang,

G.L., Liu, G.B., Mu, X.M., Li, Z.B., Li, S.Q., Yang, Y.Z., Wang, J., Xiao, X.M., 2016. Multiple afforestation programs accelerate the greenness in the 'Three North' region of China from 1982 to 2013. Ecological Indicators 61, 404-412.

Zhang, D.J., Jia, Q.Q., Xu, X., Yao, S.B., Chen, H.B., Hou, X.H., 2018. Contribution of ecological policies to vegetation restoration: A case study from Wuqi County in Shaanxi Province, China. Land Use Policy 73, 400-411.

Zhang, Y., Yuan, J., You, C.M., Cao, R., Yang, W.Q., 2020. Contributions of National Key Forestry Ecology Projects to the forest vegetation carbon storage in China. Forest Ecology and Management 462, 117981.

Zheng, H.R., Wang, Y.Q., Chen, Y., Zhao, T.Y., 2016. Effects of large-scale afforestation project on the ecosystem water balance in humid areas: An example for southern China. Ecological Engineering 89, 103-108.

Zhu, Y.K., Zhang, J.T., Zhang, Y.Q., Qin, S.G., Shao, Y.Y., Gao, Y., 2019. Responses of vegetation to climatic variations in the desert region of northern China. Catena 175, 27-36.

Author Contributions

Duanyang Xu: Conceptualization. **Daoli Peng:** Methodology. **Yue Zhang:** Data curation. **Ziyu Wang:** Writing- Reviewing and Editing.

Declaration of competing interest

The authors declare that they have no known competing financial interests or personal relationships that could have appeared to influence the work reported in this paper.

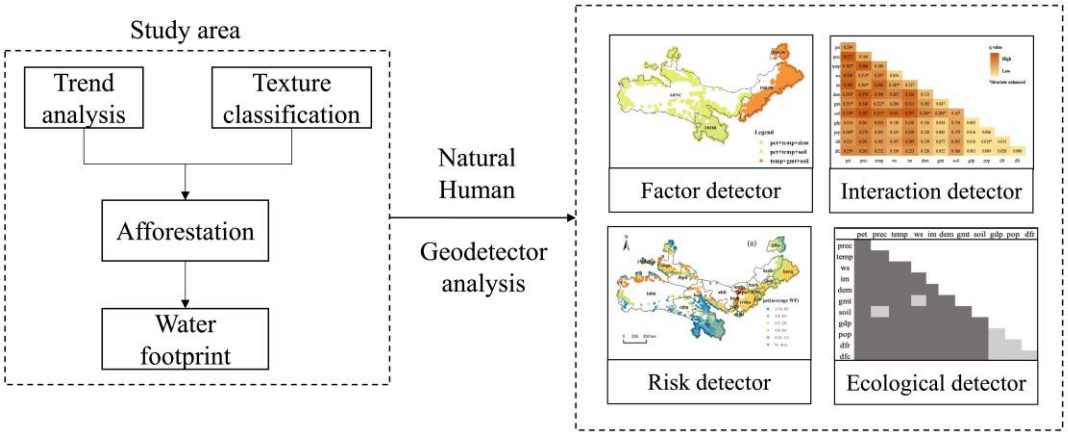

Graphical abstract

Highlights

- Afforestation area increased by 73,764.31 km^2 in sandy regions of northern China, from 2003 to 2017.
- Afforestation water footprint (AWF) showed high heterogeneity and ranged from 0 to 58.9 m^3/gC.
- Potential evapotranspiration dominated AWF at national scale but major factors differed at sub-region level
- The interactions between different factors had higher impact on AWF than single factor.